Experimental and Numerical Investigation of the Dynamics of Loop Seals in a Large-Scale DFB System Under Hot Conditions

Anton Larsson and Henrik Thunman
Div. of Energy Technology, Dept. of Energy and Environment, Chalmers University of Technology, SE-412 96 Goteborg, Sweden

Henrik Ström
Div. of Energy Technology, Dept. of Energy and Environment, Chalmers University of Technology, SE-412 96 Goteborg, Sweden

Div. of Fluid Dynamics, Dept. of Applied Mechanics, Chalmers University of Technology, SE-412 96 Goteborg, Sweden

Srdjan Sasic
Div. of Fluid Dynamics, Dept. of Applied Mechanics, Chalmers University of Technology, SE-412 96 Goteborg, Sweden

DOI 10.1002/aic.14887
Published online June 4, 2015 in Wiley Online Library (wileyonlinelibrary.com)

The dynamics of the loop seals in a large-scale dual fluidized bed (DFB) system is investigated as a function of variations in the flux of the bed material through the seal and changes in the bed material density. These investigations are performed numerically with a computational fluid dynamics (CFD) model and experimentally for the loop seals of the Chalmers 2–4 MW_{th} DFB gasifier. Both experiments and simulations show that more of the aeration gas leaves the loop seal in the direction of the solids when a low-density bed material (silica) is used rather than a high-density one (bauxite). The simulations also reveal homogeneous fluidization in a vertical connection to the loop seal, whereas an inclined connection yields heterogeneous fluidization. The minor discrepancies between the experiments and simulations with silica are attributed to particle agglomeration, and it is proposed that CFD models applied to loop seals should account for this phenomenon. © 2015 American Institute of Chemical Engineers *AIChE J*, 61: 3580–3593, 2015
Keywords: fluidization, particle technology, particulate flows, computational fluid dynamics, energy

Introduction

In a fluidized bed reactor, solid particles are used as the bed material, typically to act as a heat carrier. The particles in the bed material are perfused with gas to create a fluidized bed, in which the particles exhibit a fluid-like behavior that results in good mixing properties. There exist different fluidized bed applications, such as circulating fluidized bed (CFB) combustion and gasification,[1] as well as dual fluidized bed (DFB) systems,[2] for example, DFB gasification,[3,4] fluid catalytic cracking, and chemical looping combustion.[5] Figure 1 provides schematic presentations of CFB and DFB systems in which solid particles, for example, silica sand or a catalyst, are used as the bed materials.

In a CFB combustor, the bed material is fluidized by air in the primary reactor [(1) in Figure 1] and entrained and transported to the cyclone (2) where the solids are separated from the gas. The solids are then returned to the lower part of the primary reactor (4). To prevent the gas from migrating from the high-pressure zone in the lower part of the primary reactor to the lower-pressure zone in the cyclone through the return leg, a loop seal or return valve is required (3). The loop seal allows solids to pass while gas is prevented from passing through the return leg by introducing a pressure drop that corresponds to the pressure drop across the reactor. By adding an aeration gas to the bottom of the loop seal, the bed material becomes fluidized and flows through the loop seal (Figure 2). In DFB applications, two loop seals are required to prevent the exchange of gases between the primary and the secondary reactors (5). Thus, loop seals are vital for many processes that use a CFB or a DFB, in that they provide an appropriate pressure drop and prevent carryover of gas. Furthermore, loop seals may also be designed for additional purposes, such as heat or mass transfer or chemical reactions,[6,7] which entails more complex design and/or operation, for example, via the use of more than one aeration gas and more than one outlet.[6] In the process of retrofitting existing reactor systems with new loop seals, there might also be significant constraints on the space available for the seals that must be accounted for in the

Correspondence concerning this article should be addressed to H. Ström at henrik.strom@chalmers.se.

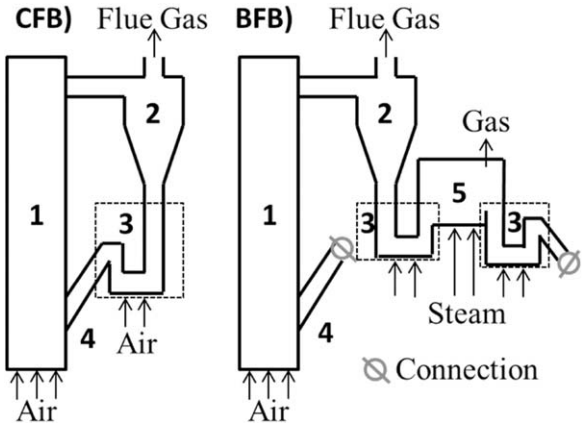

Figure 1. Schematics of a CFB system and a DFB system showing the: (1) primary reactor; (2) cyclone; (3) loop seals; (4) return leg; and (5) secondary reactor.

design process. Consequently, for optimal design and operation of the loop seals, it is necessary to devise a reliable method for predicting the flows of solids and gases inside a loop seal.

The importance of loop seals has led to several investigations that have focused on the use of loop seals for both CFB[8–13] and DFB[14–16] applications. Operational parameters that should be considered in the design of the loop seal include: the mass flow of solids, the pressure drop between the vessels connected by the loop seal, and the properties of the bed material.[13,17]

It has been shown that the flow of solids through a loop seal is restricted by the frictional forces that occur between particles, as well as those between the solids and the loop seal construct. The frictional forces between the particles are a function of the aeration of the solids, which is essential to facilitate the function of nonmechanical valves in controlling the mass flow of solids by adjusting the volumetric flow rate of aeration gas. At a certain level of aeration, any further increase in the rate of aeration has no significant impacts on the mass flow of solids and on the pressure drop, which becomes independent of the aeration level.[8,11–13,15] The pressure drop over the nonmechanical valve then automatically adjusts itself to the pressure difference in the loop, thereby forming a pressure seal that is referred to as a "loop seal." Thus, to ensure loop seal function, the aeration of the loop seal must be maintained above a certain level to ensure that the loop seal adjusts when the pressure fluctuates. This level is affected by the properties of the particles in the bed material, whereby larger particles and/or a greater density of the particles require a higher rate of aeration.[13]

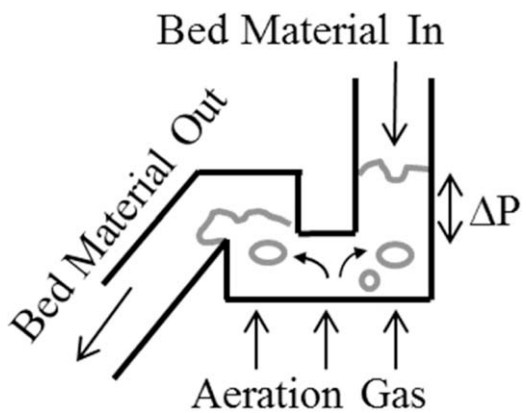

Figure 2. Illustration of a loop seal that is fluidized by an aeration gas.

The term ΔP indicates the effect of a pressure difference across the loop seal.

One of the main purposes of a DFB system is to separate the gas streams that are generated in the primary and secondary reactors.[14–16] Thus, the aim with such a system is to operate the loop seals without any gas leakage between the reactors. Problems related to gas leakage or carryover of gas through loop seals have been addressed in several studies,[8–10,13–16] indicating an association between decreased carryover and higher aeration. However, a high rate of aeration is related to high-level steam consumption or high-level power consumption if air or flue gas is used for aeration. High-level aeration can also cause slugging fluidization, which results in pressure fluctuations and attrition in the loop seal and should therefore be avoided.

For a DFB gasification system, the gas split in the loop seals is of particular importance for quantification of the steam-to-fuel ratio (SFR), which relates the total amount of steam added to the process to the amount of dry fuel. As the SFR of a gasifier affects the fuel conversion, it is important to know the gas split values of the loop seals when evaluating a DFB gasification system.[18]

Previous investigations of loop seals were based on measurements made in experimental models under cold conditions. In rare instances,[14,19] the Glickman's scaling laws[20] have been applied to mimic the temperatures actually used in CFB and DFB applications. More importantly, both Mayer et al.[14] and Lind[19] concluded that, even with the use of thermodynamic scaling, discrepancies remained between the results of the model of the cold system and the validation results from the hot system. In addition, the computational fluid dynamics (CFD) modeling used previously was either two-dimensional (2-D) or based on the multiphase particle-in-cell (MP-PIC) method.[21] However, the design of a typical loop seal does not warrant a reduction in dimensionality from three to two, and the employment of the MP-PIC method is associated with important theoretical challenges. For example, if too fine grids are used, statistical noise will influence the results.[22] In contrast, if too coarse grids are used, subgrid scale corrections must first be derived and applied.[23] In summary, the discrepancies noted between the hot and cold experimental models and the lack of fluid dynamics scaling in most of the previous experimental studies raise questions as to how well these previous results can be extrapolated to loop seals in large-scale DFB systems operating under hot conditions. Therefore, the accuracy and reliability of previous CFD modeling validated using these cold models remain uncertain. The elucidation of how a specific loop seal design is affected by operational changes (e.g., choice of bed material, solids flow rate, and pressure drops) requires comprehensive CFD modeling, which is subsequently validated by experiments in a large-scale unit operated under hot conditions.

In the present work, a three-dimensional (3-D) CFD model of a loop seal is established and used to investigate the aeration gas split, the pressure drop across the loop seal, the degree of fluidization, and the carryover of gas through a loop seal

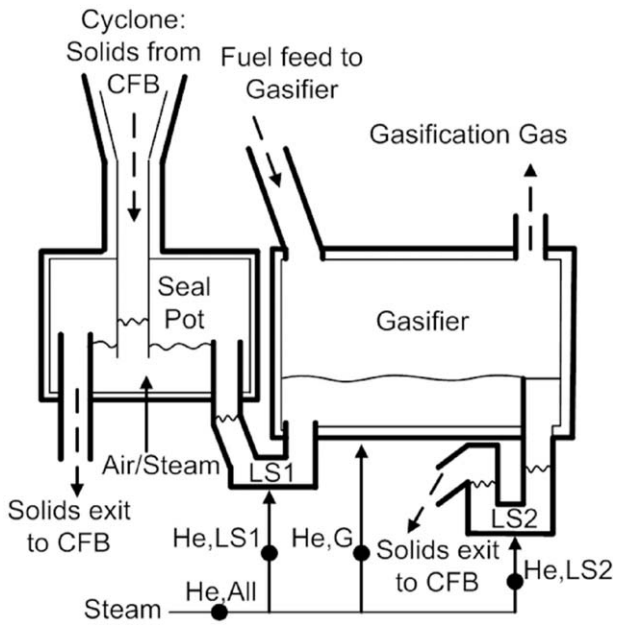

Figure 3. Schematic of the system of interest in the present work.

LS1 and LS2 represent loop seals 1 and 2, respectively. In- and out-going mass flows are indicated by arrows, and the positionings of the helium (He) injection points are indicated with dots.

during the operation of a large-scale DFB system in which different bed materials are employed. Since the focus of the work is on a DFB system, the aeration level in the loop seals is high. The computational model is validated by quantification of the gas-split and carryover of gas in the loop seals of the Chalmers 2–4 MW_{th} gasifier. It is shown how experimental data obtained under relevant conditions can be combined with comprehensive CFD modeling to provide valuable insights into the operation of a specific loop seal design.

Experimental Setup and Procedure

The experimental setup of the Chalmers system comprises a DFB gasifier (Figure 1B). The primary reactor is a 12-MW_{th}[24] CFB boiler that was retrofitted[25] with a secondary reactor, which is a DFB gasifier that is indirectly heated with the bed material from the CFB reactor.[20] The present work is focused on the loop seals that connect the loop pot of the CFB and the bubbling fluidized bed (BFB) of the gasifier (Figure 3). The bed material enters from the CFB furnace via a cyclone and is collected in a seal pot. The seal pot is a BFB with multiple exit pipes of different heights, allowing the bed material flow to be directed by enabling or disabling the fluidization of loop seal 1 (LS1) of the lower exit pipe. If LS1 is fluidized, the bed material is transported to the gasifier, and if LS1 is not fluidized, the seal pot is filled to the level of the higher exit pipe so that the bed material enters the downcomer to the CFB.[25]

The bed material that passes through LS1 enters in the bottom of the gasifier and exits over a weir section on the opposite side of the gasifier, thereby creating a cross-flow of bed material through the gasifier. The bed material exits the gasifier by passing the weir and entering loop seal 2 (LS2), such that the bed material is transported back to the CFB.

The two loop seals and the gasifier are fluidized with steam to yield a nitrogen-free gasification gas, while the CFB is fluidized with air and the loop pot can be fluidized with air, flue gas, or steam. To investigate the split of the steam in the loop seals, helium (He) is used as a tracer gas that is injected into the steam pipes (dots in Figure 3). The concentration of He in the gasification gas when He is injected into the steam duct to the gasifier (injection point He,G in Figure 3) is denoted as $C_{He,G}$. The value of $C_{He,G}$ is used as the reference concentration to establish the volume flow of gas, $\dot{V}_{gas}$, under the assumption that none of the steam (or He) added to the gasifier escapes through the loop seals. The reference concentration allows calculation of the fractions of steam that enter the gasifier from LS1, $X_{st,LS1}$, and from LS2, $X_{st,LS1}$

$$X_{st,i} = \frac{\dot{V}_{gas} C_{He,i}}{\dot{V}_{He,i}} = \frac{\dot{V}_{He,G} C_{He,i}}{\dot{V}_{He,i} C_{He,G}} \quad , i = \mathrm{LS1, LS2} \tag{1}$$

where $\dot{V}_{He,i}$ is the volumetric flow rate of injected He at point He,i. To assess the validity of the assumption that the steam injected into the gasifier (He,G) does not escape through the loop seals, two complementary experiments were performed. The fraction of the total amount of steam that entered the gasifier, $X_{st,All}$, was quantified in two ways: (1) based on the mass flow of steam, $\dot{m}_{st}$, and the fraction entering the gasifier, X_{st}, as quantified by Eq. 1; and (2) by injecting He into the main steam duct (at point He,All). The two approaches can be compared in Eq. 2 where the left-hand side of the formula is based on the first approach and the right-hand side on the second approach

$$\frac{X_{st,LS1}\dot{m}_{st,LS1} + \dot{m}_{st,G} + X_{st,LS2}\dot{m}_{st,SL2}}{\dot{m}_{st,SL1} + \dot{m}_{st,G} + \dot{m}_{st,SL2}} = X_{st,All} = \frac{\dot{V}_{He,G} C_{He,All}}{\dot{V}_{He,All} C_{He,G}} \tag{2}$$

To enable analysis of the He concentration, the gas is cooled to -2°C to remove water and tar.[18] The cooled and cleaned gas is analyzed with a molecular sieve column with argon as the carrier gas and a thermal conductivity sensor in the Agilent 490 micro gas chromatogram (GC). The GC method used enables measurements at 180-second intervals; for each investigated case, at least five measurements (~15 min) are acquired with a stable He level (standard deviation of the mean value of $<1\%_{rel}$). The purity of the injected He is 99.5% and the mass flow is controlled using a Bronkhorst mass flow controller (MFC F-202AV).

To investigate how the running of the process affects the operation of the loop seal, two major parameters are considered: (1) the mass flow of the bed material between the reactors, which is here quantified as the flux of bed material through the loop seal, and (2) the density of the bed material, which is investigated by operating the process with either silica sand or bauxite as the bed material. The operation of the loop seal is primarily characterized by the pathway that the aeration gas takes through the seal (the so-called gas split) and the extent (if any) to which the seal allows carryover of gas between the gasifier and the adjacent parts of the system.

The impact of the bed material flux on the gas split is investigated using silica sand as the bed material and by varying the level of the flux. The experiments are summarized in Table 1, where time-close experiments (conducted on consecutive days) are indicated by a mutual box. Note that the experiments are carried out in an industrial production facility and that every measurement point therefore requires a significant effort, in terms of both disruption of normal operation of the plant and substantial financial cost. The impact of the density of the bed material is investigated based on one silica sand and

Table 1. Summary of the Investigated Experimental Cases

Investigated Parameter	Flux of Bed Material Through the Loop Seal			
	84 kg/m^{2}s	93 kg/m^{2}s	99 kg/m^{2}s	112 kg/m^{2}s
Flux of bed material		×	×	×
		×	×	
	×		×	
Bed material density				
High			× (Bauxite)	
Low			× (Silica sand)	

Time-close experiments are indicated by a surrounding box.

one bauxite case, while all the other parameters are kept constant as much as possible. Particles of similar size were used (see Table 2), and the size was quantified for particles sampled from the process during the operation, so as to derive an accurate value for the particle diameter, as it might change over time.

All the investigated cases had the same level of aeration. The level of aeration is based on experimental experience (>1800 h) of running the process with a steady flow of silica sand as the bed material.

Modeling

Mathematical model

There exist today a variety of discrete particle models,[26,27] in which the Newtonian equations of motion are solved for each particle. Although these models potentially allow a very accurate description of the particle motion, they are prohibitively expensive for industrial-sized problems. In addition, if the computational efficiency of a discrete particle method is increased by a coarsening of the mesh for the continuous phase, information on the local flow field around the particle is lost and the quality of the prediction of the instantaneous drag force deteriorates.[28] Given the large number of particles that are physically present in the system of interest (the volume of LS1 in Figure 3 is approximately 0.2 m^3, which means that it contains more than 10^9 particles) and the significance of particle-particle interactions for the hydrodynamics of fluidization, the Euler-Euler (two-fluid) model is used for the numerical simulations. In this model, a statistical averaging is performed of the governing equations that describe the behavior of the particles, so that both phases are described as interpenetrating continua. A consequence of this procedure is that the interfacial terms and stress tensors require closure modeling, for which the kinetic theory of granular flow is employed. With this approach, the concept of granular temperature is introduced as a measure of the kinetic energy of the random motion of the particles. Details of the derivation of these equations are available in the literature,[29,30] and the particular implementation used in this work is shown in Table 3.

The boundary conditions applied are the specified velocities of steam at the steam injection nozzles and specified pressures at the cross-sections of the downcomer and gasifier legs (Figure 3). As the steam injection nozzles are fully resolved in the computational mesh, no additional assumptions are needed regarding the inlet distribution of the steam. The pressure outlet boundary conditions allow temporary backflow to occur, as dictated by continuity. In such cases, only steam (not particles) is assumed to flow over these boundaries. Rationalization for this choice of boundary condition will be provided later. The walls have no-slip boundary conditions and gravitation acts in the downward direction.

Particles are introduced into the loop seal by the addition of a source term in the solid-phase continuity equation in a spherical region of 1.77 dm^3 (corresponding to 19,064 computational cells) approximately 2 dm below the outlet boundary of the downcomer leg (cf. Figure 4). The size and location of the inlet region is chosen so that the incoming solids do not interact directly with the pressure outlet boundary or with the wall boundaries, while maintaining a local volume fraction of solids in the spherical region below 0.30 at all times. The bed material introduced in this way is allowed to accelerate due to gravity and fall down onto the top of the bed in the seal below. The use of source terms in this manner ensures that the correct solids flux is obtained without any need to specify otherwise-unknown boundary conditions for the solids flow at the upper boundary of the downcomer leg. Consequently, the effects of the specification of the solid-phase inlet condition on the fluidization behavior in the loop seal is deemed negligible.

Numerical considerations

Two-dimensional simulations can potentially be used to deduce information about the approximate qualitative behavior of a system, although they are often motivated primarily by a lack of available computational resources. Previous studies on simulations of the gas-solid flow in loop seals using the two-fluid model have typically dealt with 2-D simulations.[15,39] However, the hydrodynamics of the gas-solid flow is not the

Table 2. Physical Properties of Gases and Solids

Solids	Density (kg/m^3)	Surface-Weighted Mean Diameter (μm)	
Silica sand	2600	298	
Bauxite	3300	305	
Gases	**Density (kg/m^3)**	**Mass Diffusivity (m^2/s)**	**Purity**
Steam	0.197		
Helium		1.27×10^{-4}	Detector quality, 4.6

Table 3. Summary of Equations Used in the Mathematical Model

Solid phase continuity	$\frac{\partial}{\partial t}(\alpha_s\rho_s)+\nabla\cdot(\alpha_s\rho_s u_s)=0$
Gas phase continuity	$\frac{\partial}{\partial t}(\alpha_g\rho_g)+\nabla\cdot(\alpha_g\rho_g u_g)=0$
Solid phase momentum balance	$\frac{\partial}{\partial t}(\alpha_s\rho_s u_s)+\nabla\cdot(\alpha_s\rho_s u_s u_s)=-\alpha_s\nabla p-\nabla p_s+\nabla\cdot\tau_s+\alpha_s\rho_s g+K_{gs}(u_g-u_s)$
Gas phase momentum balance	$\frac{\partial}{\partial t}(\alpha_g\rho_g u_g)+\nabla\cdot(\alpha_g\rho_g u_g u_g)=-\alpha_g\nabla p+\nabla\cdot\tau_g+\alpha_g\rho_g g+K_{sg}(u_s-u_g)$
Granular temperature[31]	$\frac{3}{2}\frac{\partial}{\partial t}(\alpha_s\rho_s\Theta_s)=(-p_s I+\tau_s):\nabla u_s-\frac{12(1-e_{ss}^2)g_{0,ss}}{d_s\sqrt{\pi}}\alpha_s{}^2\rho_s\Theta_s{}^{3/2}-3K_{gs}\Theta_s$
Interphase exchange coefficient[32]	$K_{sg}=\frac{3\alpha_g\alpha_s\rho_g}{4u_{r,s}^2 d_s}C_D\frac{Re_s}{u_{r,s}}\lvert u_s-u_g\rvert, with^{33}: C_D=\left(0.63+\frac{4.8}{\sqrt{Re_s/u_{r,s}}}\right)^2 and^{34}:$
	$u_{r,s}=0.5\left(\alpha_g^{4.14}-0.06Re_s+\sqrt{(0.06Re_s)^2+0.12Re_s\left(2B-\alpha_g^{4.14}\right)+\alpha_g^{8.28}}\right)$
	$B=\begin{cases}0.8\alpha_g{}^{1.28}, & \alpha_g\le 0.85\\ \alpha_g^{2.65}, & \alpha_g>0.85\end{cases},\quad Re_s=\frac{\rho_g d_s\lvert u_s-u_g\rvert}{\mu_g}$
Solids pressure[35]	$p_s=\alpha_s\rho_s\Theta_s+2\rho_s(1+e_{ss})\alpha_s^2 g_{0,ss}\Theta_s$
Radial distribution function[35,36]	$g_{0,ss}=\left[1-\left(\frac{\alpha_s}{\alpha_{s,max}}\right)^{1/3}\right]^{-1}$
Solid phase shear stresses	$\tau_s=\alpha_s\mu_s(\nabla u_s+\nabla u_s{}^T)+\alpha_s\left(\lambda_s-\frac{2}{3}\mu_s\right)\nabla\cdot u_s I$
Solid phase shear viscosity	$\mu_s=\mu_{s,col}+\mu_{s,kin}+\mu_{s,fr}$
Solid phase collisional viscosity[31,37]	$\mu_{s,col}=\frac{4}{5}\alpha_s\rho_s d_s g_{0,ss}(1+e_{ss})\left(\frac{\Theta_s}{\pi}\right)^{1/2}$
Solid phase kinetic viscosity[31]	$\mu_{s,kin}=\frac{\alpha_s\rho_s d_s\sqrt{\Theta_s\pi}}{6(3-e_{ss})}\left[1+\frac{2}{5}(1+e_{ss})(3e_{ss}-1)\alpha_s g_{0,ss}\right]$
Solid phase frictional viscosity[38]	$\mu_{s,fr}=\frac{p_s\sin\phi}{2\sqrt{I_{2D}}}$
Solid phase bulk viscosity[35]	$\lambda_s=\frac{4}{3}\alpha_s\rho_s d_s g_{0,ss}(1+e_{ss})\left(\frac{\Theta_s}{\pi}\right)^{1/2}$

same in a 2-D simulation as in the corresponding 3-D case.[40,41] We thus believe that the loop seal of interest in the present work can only be accurately represented by a 3-D geometry (Figure 4).

The equation set formed by the mathematical model is solved in a finite volume framework using a pressure-based, segregated solver on a colocated grid. The phase-coupled SIMPLE algorithm is used for the pressure-velocity coupling,[42] and the time discretization of all equations is first-order implicit. The first-order upwind scheme is used to satisfy boundedness for the spatial discretization of the advective term in the particle volume fraction equation (obtained from the solid-phase continuity equation). The gas-phase volume fraction is obtained from the condition that the two volume fractions always should sum to unity.

The decision to specify the volume fraction of solids as zero in the event of backflow over the outlet boundaries is motivated by several important considerations. First, the sizes of the reactors are such that the full DFB system (cf. Figure 1) cannot be simulated in its entirety, given the long simulation times needed to gather statistical data (as will be discussed further in the next section). Thus, the appropriate boundary

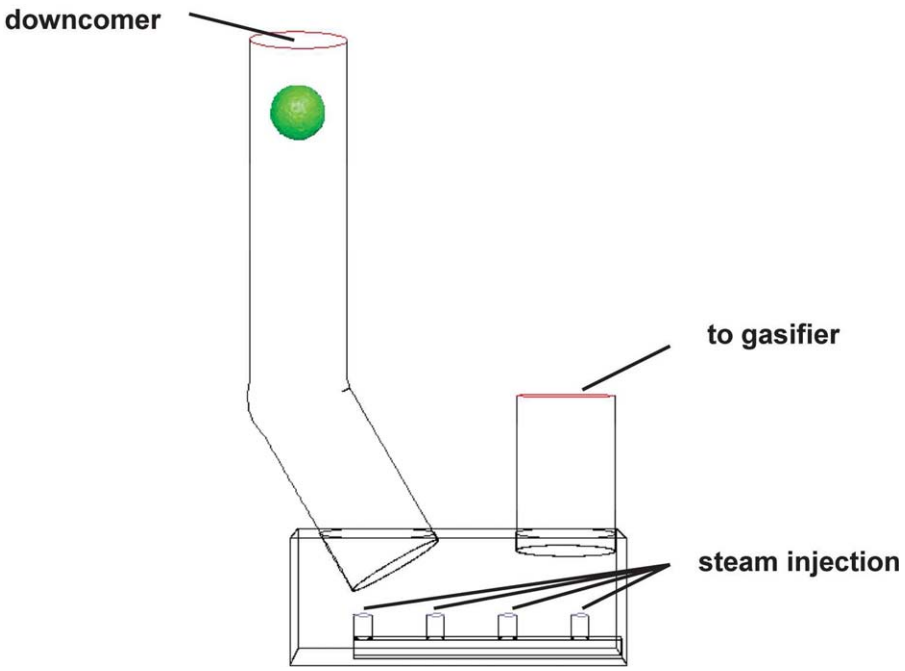

Figure 4. Outline of the three-dimensional computational domain.

The green sphere illustrates the region where the solids are introduced via source terms. The computational mesh contains approximately 2.5 million cells. [Color figure can be viewed in the online issue, which is available at wileyonlinelibrary.com.]

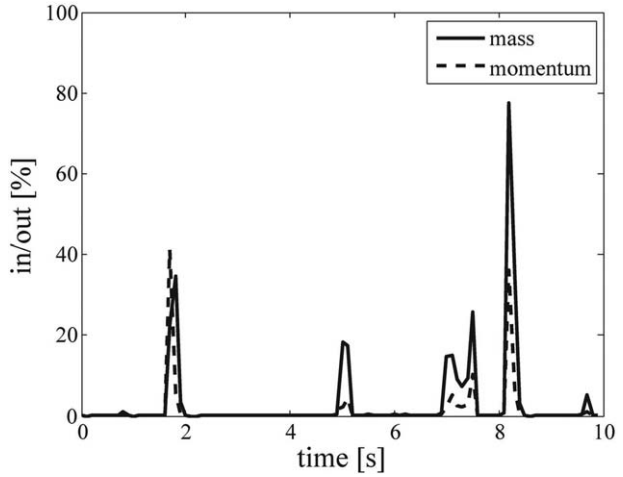

Figure 5. Time-resolved ratios of the incoming to the outgoing mass and momentum flow rates over the outlet to the gasifier in the simulations with bauxite.

conditions for solid-phase backflow (e.g., in terms of volume fraction, velocities, and granular temperature) are by definition unknown in the simulations of the loop seal. Re-entry of solids from the gasifier leg, the properties of which have been specified *a priori*, would influence the dynamics of the gas-solids flow in that part of the system in ways that would be difficult to quantify. Furthermore, such a backflow of solids would also necessarily affect the solids flux, making it difficult to perform relevant comparisons between the experiments and simulations. Finally, allowing only steam to flow back over the outlet boundaries acts to increase the carryover of gases between the two legs of the seal, so that the carryover is not underestimated in the simulations. Nevertheless, the effect of the applied outlet boundary condition in the gasifier leg was also quantified by analysis of the behavior of the solution variables over the boundary. Figure 5 illustrates the time-resolved ratio of the incoming to the outgoing mass and momentum flow rates over this outlet. It can be seen that the influence of backflow over the boundary is very small most of the time, with only a few intermittent peaks. Furthermore, an estimate of the depth of influence from the backflow was obtained using a theoretical model for spray penetration.[43] With this method, the backflow is described as a spray originating from the cell face on the boundary over the duration of the time step and with the same total momentum flux as the backflow in question. If the spray cone angle was taken to be 22.5° (a reasonable assumption for a high-pressure spray discharging into a quiescent atmosphere), the time-average of the calculated penetration depth was 13.6 ± 10 mm and the maximum penetration depth in each time step was 75.9 ± 32 mm. This depth represents only a minor section of the leg connected to the gasifier, which has a total height of 720 mm measured from the bottom floor of the loop seal. These calculations therefore support the conclusion that the influence of the backflow on the flow field inside the loop seal, and on the quality of the fluidization in the leg leading to the gasifier, is limited to a relatively small region close to the boundary.

Analysis of the gas split signal from the model

The main parameter of interest in the numerical simulations is the split signal, defined as the ratio of the mass of the steam that exits to the gasifier to the total mass of steam injected into the loop seal. A time-averaged value of this signal is obtained by time integration of the instantaneous mass fluxes of steam and the subsequent calculation of the appropriate ratio.

Three-dimensional numerical simulations of fluidized gas-solid systems are computationally expensive to perform[44] (CPU-to-real-time ratios in the order of 10^5-10^6), which restricts the duration of the time signals that can be obtained for subsequent analysis.[40,41,45,46] The computational cost is further increased if the influences of different operating conditions for the loop seal are to be examined. In the present work, two of the experimental cases [with high-density (bauxite) and low-density (silica) bed materials] are chosen for further numerical investigation. Each simulation is performed in parallel mode using 32 Nehalem CPUs (Xeon E5520, 2.27 GHz).

It is customary to exclude the first 5–10 s of the simulated data in the analysis, to prevent any influence of the initialization or the startup phase, and to gather data for the signal analysis until the sampling of the investigated variable converges. In practice, sequences as short as 4 s have been used for 3-D simulations, whereas longer sequences may be used for 2-D or laboratory-scale systems.[40,41,45,46] Gel et al.[47] performed a comprehensive validation and uncertainty quantification investigation of a CFB simulation setup and found that the spatial discretization error was the predominant source of uncertainty, far outweighing the influence of the time averaging error. Therefore, we choose to obtain spatially well-resolved solutions for affordable time periods rather than the opposite (i.e., under-resolved solutions for longer sampling times). The spatial resolution is thus everywhere in the domain much finer than the threshold defined by Cloete et al.[44] for grid-independent phase-segregation and grid-independent reactor performance. The smallest and largest computational cells have sides equal to 0.35 mm and 6.9 mm, respectively. In this work, the first 11.6 s of the signal were discarded, and the sampled values converged after an additional 11.4 s for the bauxite case and 6.6 s for the silica case. Convergence of the sampled value is judged by monitoring the ratio of the absolute change in the sample value between two successive samples to the largest change observed during the sampling. The relative change defined in this way had to decrease by more than three orders of magnitude during the total sampling time for the signal to be considered as having converged. The time series for the convergence of the monitored split signals for the bauxite case is shown in Figure 6.

Due to the fine temporal resolution in the numerical simulations, high-frequency fluctuations in the split signal are captured and have to be dealt with in the signal analysis. More specifically, the standard deviation of the split signal remains significant (of the order of 30% for both cases) when the accumulated mean value has converged. Consequently, even with converged mean values, it is still a delicate task to differentiate with high statistical significance the trends for different operation points for the loop seal.

In an attempt to acquire additional information regarding the trend for the split signal with respect to the pressure drop across the gasifier bed, an alternative trend-probing methodology was developed and employed. A complete instantaneous solution to one of the cases (i.e., the silica or the bauxite case) is carried out and used as the starting point for a simulation of the other case (with different material properties and boundary conditions). The difference in evolutions between the split signals is monitored for the short period of time over which the two solutions still correlated. Here, this time period is chosen to be 0.1 s, which corresponds to approximately 1/10th of the retention time in the loop seal based on the nominal volume of

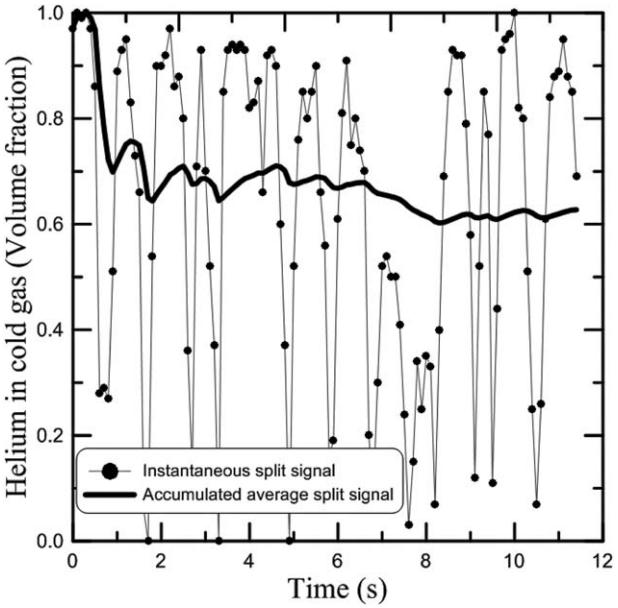

Figure 6. Time series for the convergence of the monitored split signal for the bauxite case in the numerical simulation.

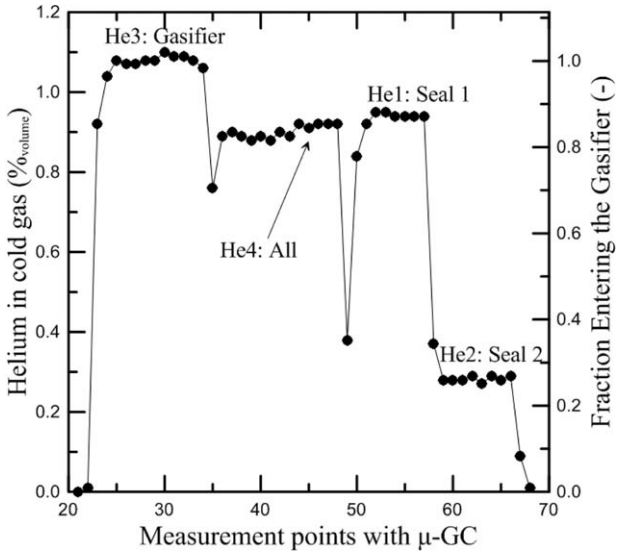

Figure 7. Measured He concentrations (left *y* axis) and the calculated fractions of steam entering the gasifier (right *y* axis), while sequentially injecting He at the various injection points.

the lower compartment, and at the same time to up to a complete passage from the nozzle tip to the outlet of the gasifier leg for the steam that is injected just below this leg. Several such comparisons for different sets of instantaneous solutions are carried out, and the switches are performed in both directions (i.e., silica case uses bauxite case solution as start-point and vice versa). The usefulness of this comparison is based on the assumption that a solution obtained with one set of boundary conditions and material properties is a good approximation of a valid instantaneous solution for a different, yet similar, set of boundary conditions and material properties. This assumption is supported by investigations of the time-averaged contour plots of the various solution fields from the two different cases. Consequently, repeated switching of the boundary conditions and material properties is valuable when establishing the expected trend. It should be stressed here that while this method does not reveal quantitative information about the magnitude of the differences in the split signal, it provides qualitative information about the relative trends for the split signal between the two cases.

Results and Discussion

The operation of the loop seals in the Chalmers gasifier is investigated both experimentally and numerically. Of particular interest is the determination of the aeration gas split, that is, the tendency for the aeration gas supplied to the loop seal to go the gasifier or to the other leg. Furthermore, we investigate the fluidization behavior inside the loop seal and how the latter affects the pressure field and the potential carryover of gas through the seal.

Experimental quantification of the gas split

To investigate the gas split in the loop seals, the concentrations of He injected into the particle seals are analyzed. Figure 7 shows the He concentrations and fractions that resulted from the injection of a known amount (50 nL/min) of He into the gasifier (He,G in Figure 3), main steam duct (He,All), loop seal 1 (He,LS1), and loop seal 2 (He,LS2). The measured He concentration in the gasification gas is used to determine the gas split using Eq. 1. The results are summarized in Table 4, where the fraction of steam supplied to the gasifier (0.85), as calculated from the right-hand side of Eq. 2, can be compared with the fraction of steam delivered to the gasifier, as calculated from the left-hand side of Eq. 2, based on the fractions of steam entering the gasifiers from the loop seals (0.87). The results are in good agreement, which means that it is valid to assume that all the He injected into the gasifier ends up in the gas that exits the gasifier.

Furthermore, the potential carryover of gas (air) from the seal pot was investigated by switching the fluidization media

Table 4. Total Amounts of Steam Entering the Gasifier, Calculated Based on Injections Made to the Loop Seals (Eq. 1) and Compared to the Total Amounts of Steam Entering the Gasifier, Which are Based on the Levels of He Injected into the Main Steam Duct (Eq. 2)

Injection Point	Gasifier (He, G)	Main Duct (He, All)	Loop Seal 1 (He, LS1)	Loop Seal 2 (He, LS2)	All (Eq. 2)
Steam flow (kg/h)	211	300	45	44	300
He concentration (Vol %)	1.082 (9)	0.918 (4)	0.943 (5)	0.283 (8)	–
Calculation of the steam fraction	Reference level	Right-hand side of Eq. 2	Eq. 1	Eq. 2	Left-hand side of Eq. 2
Steam fraction to gasifier (fraction of He)	1	**0.85**	0.86	0.26	**0.87**

The compared values are highlighted in bold text.

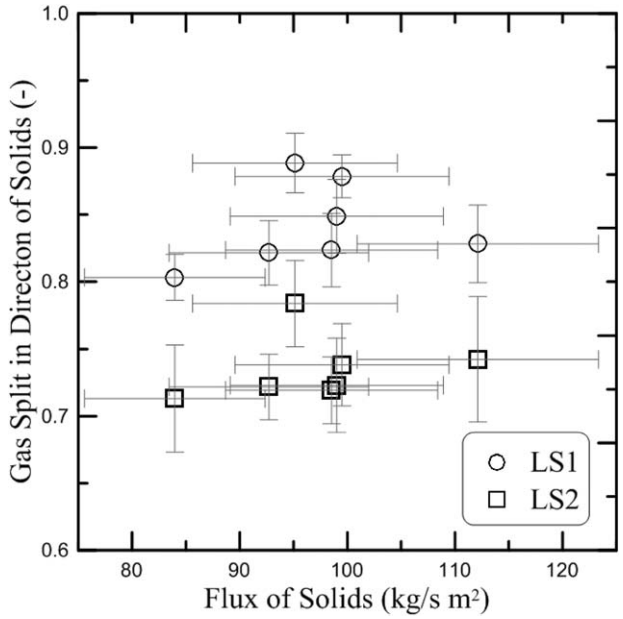

Figure 8. Gas split in the loop seals as a function of the flux of solids.

The vertical error bars represent the combined standard deviation from the He measurements in each point, whereas the horizontal error bars illustrate the experimental uncertainty in the determination of the solids flux (within 10%) as validated in our previous work.[18]

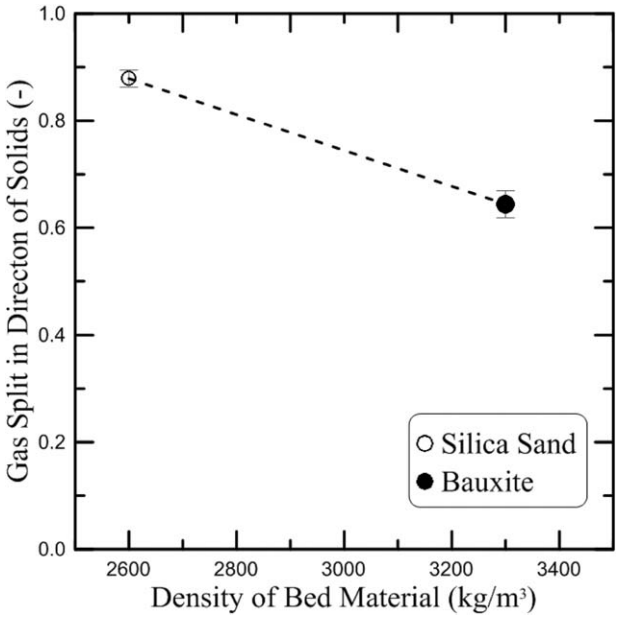

Figure 10. Gas split in the loop seals as a function of the density of the bed material.

The dotted line is a linear fit, included solely for illustrational purposes. The error bars represent the standard deviation in the experimental measurements.

from air to steam in the seal pot and monitoring the level of nitrogen in the gasifier. No significant change in the nitrogen level was detected at any time-point, which confirms that no carryover of gas occurs through loop seal 1. This proves that the measured concentrations of He in the gas from the gasifier can be used in Eq. 1, as proposed.

The results from the experiments show that changes in the flux of the bed material through the loop seals do not have a significant impact on the gas split in the loop seals. Figure 8 shows the split of the aeration gas as a function of the flux of the bed material. The split is expressed here as the fraction of steam that follows the direction of the solids. The experimental cases that were investigated under consecutive days are indicated with connecting lines. No significant trend is evident for either the time-close or the other cases.

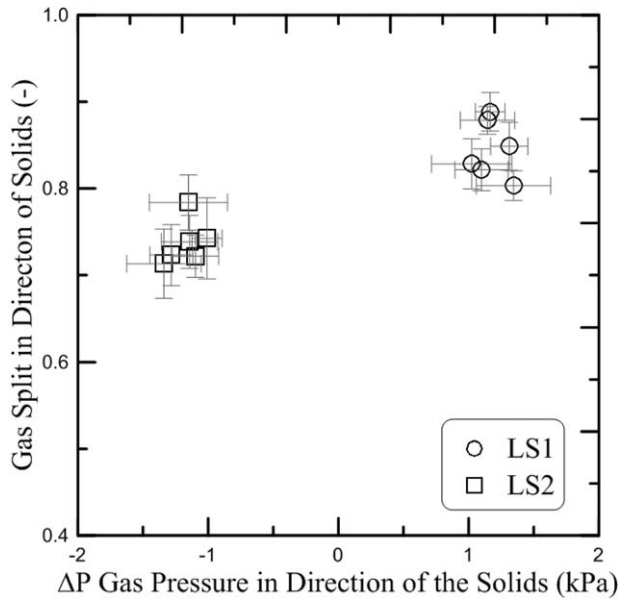

Figure 9. Gas split in the loop seals as a function of the difference in the gas pressure across the loop seals in the direction of the solids flow.

The error bars represent the standard deviation around the mean for each measurement point.

Another parameter that can affect the gas split is the difference in gas pressure between the two sides of the loop seals. Although this cannot be controlled in the current system, it can differ to some extent between cases. Figure 9 shows that the pressure difference in the gas phase between each side of the loop seal has no clear impact on the gas splits in LS1 and LS2, respectively.

Interestingly, there is a significant difference in the gas split between the two seals. This difference can be attributed to both the difference in the gas pressure across the loop seals (cf. Figure 9) and design differences. Loop seal 1 is connected to the bottom of the gasifier and the latter is part of the weir section of loop seal 1, which means that it has a considerably higher sand pillar to overcome than does loop seal 2.

In summary, these results show that the solids flux can be changed within a wide range without any significant impact on the gas split. Instead, these variations in the gas split indicate that other effects, such as aging and sintering of the bed material, affect the gas split.

LS1 is chosen for a more detailed experimental and computational analysis, as the carryover of gas has been investigated experimentally (by monitoring the nitrogen level in the gasifier) for this loop seal.

Figure 10 shows the split of gas in the direction of the solids as a function of the density of the bed material for the two investigated materials (silica sand and bauxite). There is a significant difference in the gas split for these two cases. With a low-density bed material (silica sand), a larger fraction of the aeration gas follows the direction of the bed material than

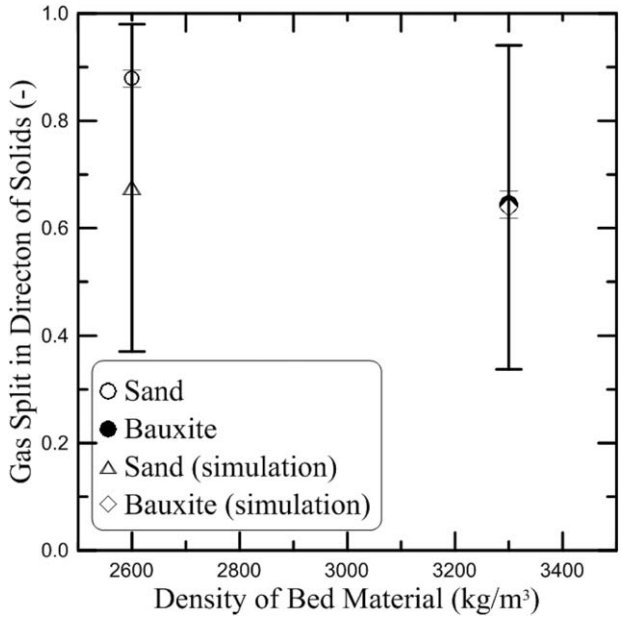

Figure 11. Gas splits in the loop seal: comparison of the results from experiments and numerical simulations.

The trend in the numerical simulations has been verified with an additional trend-probing methodology, as explained in the text. The larger error bars indicate the standard deviations of the numerical simulation. The smaller error bars represent the standard deviations in the experimental measurements.

when a high-density bed material (bauxite) is used. The bubbling bed of the gasifier represents the upper part of the weir section of LS1, and therefore, the pressure drop is higher with bauxite than with sand, with consequent lower flow of aeration gas toward the gasifier. To investigate in more detail how the exchange of bed material from silica sand to bauxite affects the function of LS1, simulations are conducted for both a bauxite case and a silica sand case.

Numerical predictions of the gas split

The numerically predicted gas splits for the two different experiments (with silica sand and with bauxite, respectively) are plotted together with the experimental data in Figure 11. The numerical (time-averaged) value for the gas split of the high-density (bauxite) bed material is in very good agreement with the experimental result. For the low-density (silica) bed material, the numerical and experimental predictions agree within the range of uncertainty provided by the standard deviation of the fluctuating numerical signal. The same trend is noted for the mean value of the split of steam with a change of bed material in both the experiments and simulations, although the magnitude of the trend is different. The newly developed trend-probing methodology reveals that the split signal in the low-density case is higher by $1.04 \pm 0.04\%$ than that in the high-density case. In other words, simulations of a higher-density bed material result in a decrease of the split signal, as compared with simulations of low-density bed material. Again, this result provides qualitative support for the conclusion that the gas split decreases when the switch is made to a bed material of higher density.

The discrepancy between the experimental and the computational results in terms of the absolute value of the trend may indicate that effects that are not captured by the present model (e.g., particle-size distribution, nonspherical particles, sintering or agglomeration of bed material,[30,48] and ash coating) can influence the split of gas in a loop seal. This conclusion is supported by the experimental observation that no significant sintering or agglomeration occurred when bauxite was used (2 weeks of operation), whereas when silica sand was used, agglomeration was detected to some extent in all the cases (1–5 weeks of operation), as evidenced in Figure 12. Thus, it is likely that the higher level of agreement between the numerical results and the experimental data seen for bauxite is because the particle properties are better characterized and constant for the bauxite case. Therefore, subsequent investigations are conducted exclusively with the bauxite bed material, to minimize the discrepancy between experiments and simulations due to sintering and aging of the bed material.

Fluidization behavior in the loop seal

Our study of the fluidization behavior in the loop seal reveals that heterogeneous fluidization takes place in the inclined entrance pipe of the loop seal, while a more homogeneous fluidization occurs in the vertical exit pipe. The heterogeneous fluidization in the entrance pipe causes pressure fluctuations and may cause attrition in the loop seal. With heterogeneous fluidization, a part of the bed material acts as a moving bed, which can entrain gas through the loop seal, resulting in carryover of the gas.

The fluidization behavior is investigated based on the volume fraction of solids and the gas velocity. Figure 13 shows the time-averaged volume fractions of solids as a contour plot across the central vertical cross-section of the loop seal. In addition, horizontal cross-sections of the inlet and the exit pipes are illustrated in the upper-right corner. Figure 13 shows zones with a high particle volume fraction in between the nozzles, as well as in the inclined inlet pipe, indicating stagnant or poorly fluidized zones. In addition, the horizontal cross-section of the inclined inlet pipe shows that a large fraction of

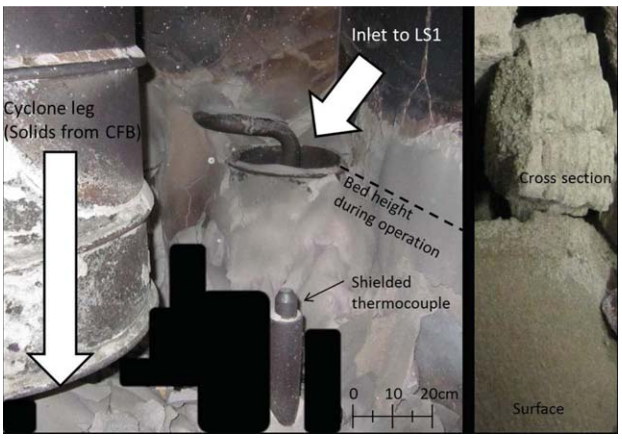

Figure 12. Photo from within the loop pot after operation with silica sand (left), taken in conjunction with the experiments reported in the present work.

Most of the bed material has been removed to expose the results of agglomeration. (Some of the nozzles present have been covered in the photo so as to not reveal their protected design). The picture to the right shows close-up examples of the agglomerated silica bed material.

[Color figure can be viewed in the online issue, which is available at wileyonlinelibrary.com.]

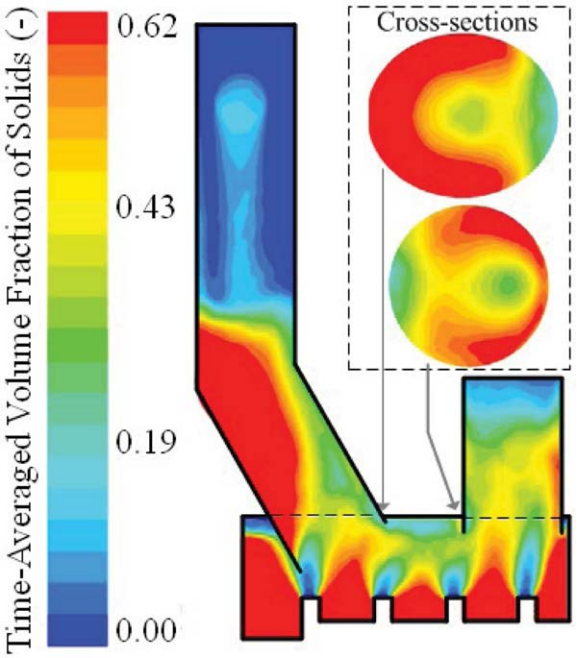

Figure 13. Contour plot of the time-averaged volume fractions of particles across the central vertical cross-section and the horizontal cross-sections of the inlet and outlet pipes.

[Color figure can be viewed in the online issue, which is available at wileyonlinelibrary.com.]

the pipe is poorly fluidized, whereas the upper section of the pipe has a low volume fraction of particles. Thus, most of the gas passes along the upper part of the inclined pipe, as expected.

The vertical exit pipe is shown to have a more even distribution of the time-averaged volume fraction of solids, albeit with more-dense regions along the walls and a region of low concentration of solids of the cross-section closest to the horizontal section of the loop seal. While a low volume fraction of solids is observed in the upper part of the exit pipe, in a real-life case, the loop seal exits into the bottom of the gasifier and this region should thus have a higher volume fraction of solids. This discrepancy is related to the definition of the boundary conditions, which states that pure steam enters from the gasifier in the case of backflow. Consequently, the upper part of the exit pipe should be disregarded in the analysis; it is shown here solely to provide a comprehensive overview of the modeling results. It is worth emphasizing that the region of lower volume fraction in the upper part of the vertical pipe is of the same depth as estimated using spray penetration theory. Furthermore, it should be noted that the zone with a volume fraction of around 0.19 in the central part of the upper section of the inlet pipe is caused by the source terms of the solids rather than being a consequence of the actual loop seal function.

The fluidization behavior in the loop seal is further studied based on the time-averaged gas velocity, as illustrated in Figure 14. Here, the minimum fluidization velocity,[1] U_{mf}, estimated for the bauxite particles, is presented on a logarithmic scale. Figure 14 shows that the averaged gas velocity in the inclined pipe is close to that of the minimum fluidization, which indicates that defluidization can occur in this section.

Carryover of gas

Despite the heterogeneous fluidization in the inlet pipe inherent to a design with an inclined pipe, the current design is efficient in avoiding carryover of gases. The potential entrainment, and thereby, the carryover of gas in the direction of the bed material (left to right), is numerically investigated by solving a convection–diffusion equation for a trace gas contained in the steam that is introduced into the loop seal. This trace gas has the same diffusivity as helium, so as not to cause an underestimation of the carryover of small and light species (heavier compounds are expected to have significantly higher diffusivities). Figure 15 illustrates the time-averages of the normalized concentration of the He tracer, where a value of 1 indicates that the He originated from the steam introduced through the nozzles, while a value of 0 indicates that the He entered from a connected vessel. The results displayed in Figure 15 reveal that the average entrainment of gas with the solids is low, and that the steam fraction entering the inclined inlet pipe is sufficient to suppress any carryover of gas. This observation is in line with the results obtained from the experiments, which show no indication of carryover of gas. However, these results are not in concordance with the findings of several studies[10,13,14] that have reported a carryover of gas. This discrepancy can be attributed to a range of issues, including ones related to the use of an inclined inlet pipe, hydrodynamic scaling, operation in hot vs. cold conditions, bed material properties, and fluidization of the particle seal. Whereas the present work is comprehensive in including both experimental results from a real system under relevant conditions and concordant numerical results from simulations of the same system, further research is needed to clarify the reasons for these differences.

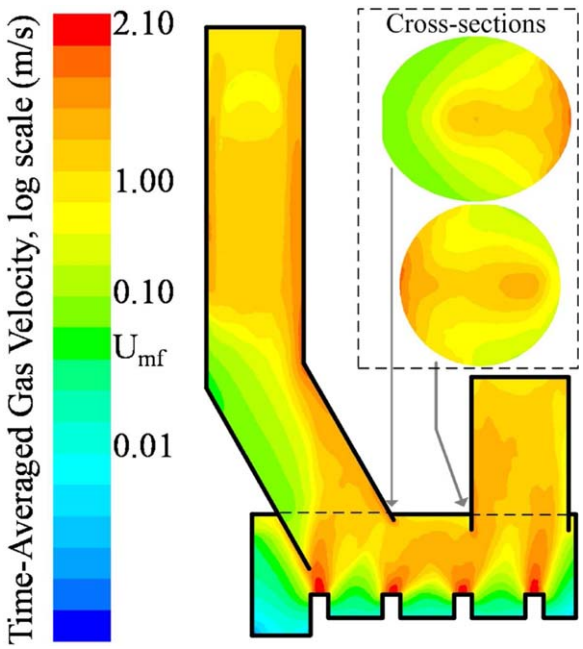

Figure 14. Contour plot of the time-averaged gas velocities across the central vertical cross-section and the horizontal cross-sections of the inlet and outlet pipes. U_{mf} = 0.043 m/s.

[Color figure can be viewed in the online issue, which is available at wileyonlinelibrary.com.]

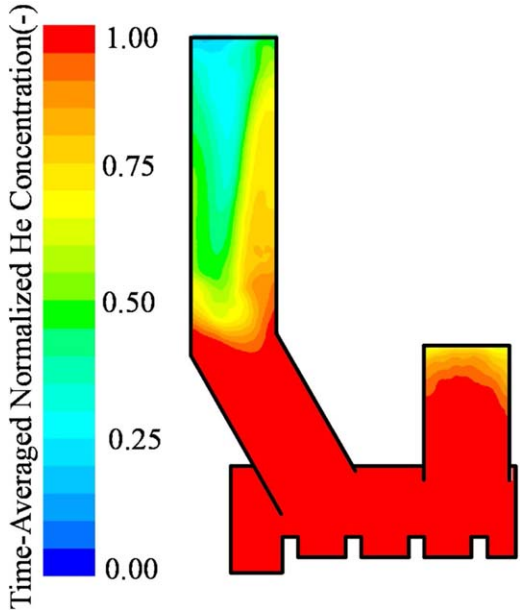

Figure 15. Contour plot of the time-averaged, normalized He concentrations across the central vertical cross-section.

[Color figure can be viewed in the online issue, which is available at wileyonlinelibrary.com.]

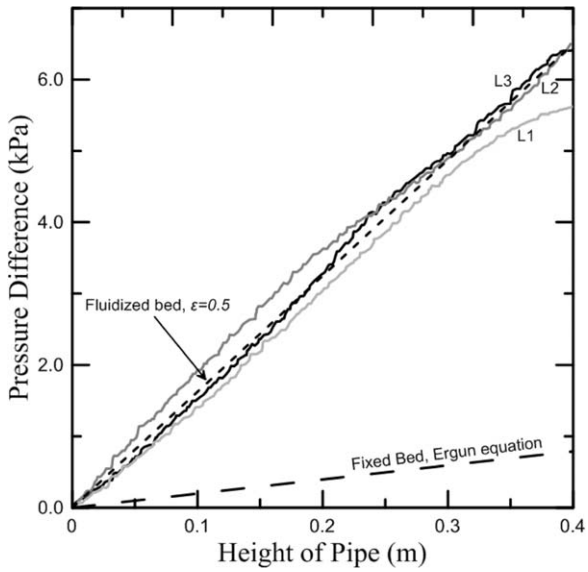

Figure 17. Pressure differences across loop seal 1 as a function of the height of the loop seal, based on the pressure along the line scans L1–L3 (indicated in Figure 16).

The results are compared with empirical correlations for fixed and fluidized beds, respectively.

Pressure of a loop seal

Although the main function of loop seals is to ensure a pressure difference between the two vessels, the vertical space available for the loop seal construct may be restricted. When designing a loop seal, an important design parameter is the heights of the inlet and outlet pipes, which must be sufficient to cope with the pressure difference between the reactors. At low aeration levels, the bed material acts as a moving bed in the inlet pipe and the pressure drop can be estimated using the Ergun equation.[1] As aeration increases, the pressure drop across the moving bed increases up to the point of fluidization, after which the pressure drop levels out. The operation and design of the loop seals investigated in the present work allow a high pressure drop that corresponds to the pressure drop across a fluidized bed with the porosity value of 0.5, as estimated by the empirical correlation of Kunii and Levenspiel.[1]

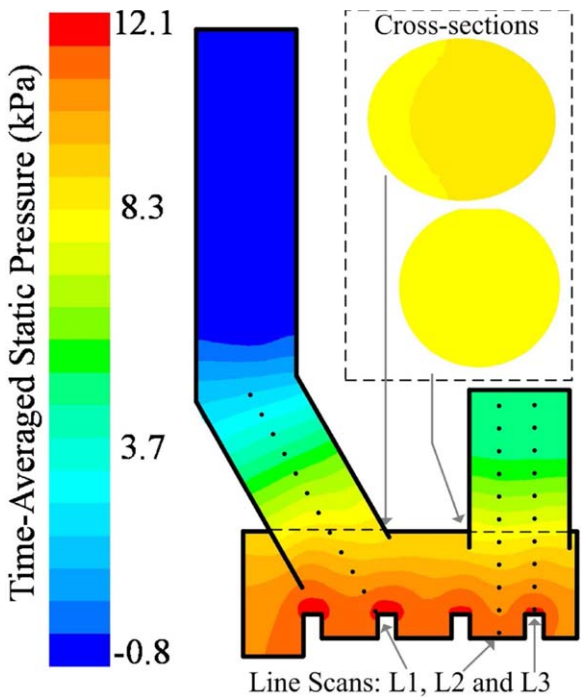

Figure 16. Contour plot of the time-averaged static pressures over the central vertical cross-section and the horizontal cross-sections of the inlet and outlet pipes, as indicated.

Line scans of the pressure (L1–L3) are indicated by dotted lines. [Color figure can be viewed in the online issue, which is available at wileyonlinelibrary.com.]

The time-averaged static pressure profile obtained from the numerical simulations is illustrated in Figure 16. The horizontal cross-section shows a heterogeneous pressure profile, with higher pressure in the sections that have a low volume-fraction of particles (cf. Figure 13). The pressure profile of the vertical exiting pipe is homogeneous with only minor variations. To investigate further how the pressure drop increases with the height of the loop seal, three line-scans (indicated as L1, L2, and L3 in Figure 16) are analyzed. Figure 17 shows the time-averaged difference between the local pressure and the pressure at the nozzles as a function of the height above the nozzles. The results from the CFD simulations are compared with empirical correlations for the pressure drop across a fluidized bed and the pressure drop across a fixed/moving bed. This shows that an assumption of a moving bed would give a substantially lower estimate of the pressure difference than the CFD model. Instead, the pressure differences agree well with those for a fluidized bed with 50% voidage. Operating a loop seal in such a way that the pressure drop resembles that of a fluidized bed could reduce considerably the required height for a specific loop seal, and the results show that the current loop seal supports a compact design in the vertical direction. Furthermore, these results highlight the usefulness of a comprehensive mathematical model in the evaluation of a specific loop seal design.

Conclusions

The functions of a loop seal in a DFB system are investigated for a large-scale loop seal operated under hot conditions. The investigations are carried out using detailed experiments (pressure signal measurements and trace gas addition) and using Eulerian-Eulerian CFD simulations. The operation of the loop seal is characterized based on the pathway taken by the aeration gas that passes through the seal (the so-called "gas split") and the degree of carryover of gas through the seal. The following conclusions are drawn from the present study:

- The investigated loop seals show robust performance with little variation in the gas split for a wide range of bed material fluxes (83–113 kg/m^{2}s).
- The density of the bed material particles significantly affects the gas split. Our results show that 80–89% of the steam used for fluidization of a loop seal follows the direction of the solids when low-density particles (2600 kg/m^3) are used, while approximately 65% of the steam used for fluidization of the loop seal follows the direction of the bed material when high-density particles (3300 kg/m^3) are used.
- The association between the gas split and the density of the bed material can be described by the mathematical model by accounting for the differences in particle properties and boundary conditions. The experimental and numerical results are in good agreement for high-density particles (bauxite case). For low-density particles (silica case), the results show agreement, although there are uncertainties related to the duration of the sampling applied in the numerical simulation; the difference between the mean signal and the experimental signal is greater than that observed for the high-density particles. As particle agglomeration is detected in the silica sand experiment (but not in the bauxite experiment), and bearing in mind that such phenomena are not accounted for in the model, agglomeration is proposed as the main mechanism behind these discrepancies (and thus, is a mechanism of relevance for the gas split).
- A new, qualitative trend-probing methodology is proposed for numerical comparisons between different operating conditions and bed materials, and the analyses using this methodology agree with the experimental data. This methodology has the potential of offering qualitatively correct estimations of the trends in the behavior of fluidized bed systems as a function of changes to the operating conditions and/or bed material, and its performance will be investigated for other types of fluidized systems in our ongoing work.
- Time-averaged results from the numerical simulations show that the inclined inlet pipe for the loop seal causes heterogeneous distribution of the gas velocity and volume fraction of particles over the horizontal cross-section, with partially defluidized regions as a consequence. In contrast, the horizontal cross-section of the vertical exit pipe is homogeneously fluidized. For loop seal designs similar to the present one, in terms of the relative locations of the pipes and the steam injection nozzles, use of vertical pipe connections is deemed more robust.
- The simulated pressure drop over the loop seal agrees well with the empirical description of the pressure drop over a fluidized bed, showing that a high pressure-difference over the loop seal can be achieved with a relatively compact loop seal.
- The carryover of gas through the loop seal is completely avoided in the investigated loop seal, as shown by the modeling results and validated by the experimental results. Thus, even though the design of the loop seal results in heterogeneous fluidization across the horizontal cross-section in the inlet, the carryover of gas is successfully avoided.

In conclusion, loop seals are vital for circulating fluidized bed and DFB processes, in that they provide an appropriate pressure drop and prevent carryover of gas. More complex loop seal designs are also used for other purposes, such as accomplishing enhanced heat and mass transfer or chemical reactions between the different streams of gases and solids in the process. Consequently, for optimal design and operation of the loop seals, it is necessary to have a reliable method for predicting the gas-solid flow inside a loop seal. The main contribution of the present work is the use of a detailed experimental characterization of two loop seals in a real large-scale DFB system operating under hot conditions to validate a herein proposed mathematical model for numerical predictions of this gas-solid flow. For a bed material that does not exhibit significant agglomeration with time, the present model can be used directly to predict the influence of the operational parameters and the loop seal design on the dynamics of the flow. Hence, the design of new loop seals for other scales or processes can be prototyped via the use of the proposed computational model. For a bed material for which significant agglomeration takes place, it is proposed that the model applied to the gas-solid flow in the loop seals should first be extended to account for this phenomenon.

Acknowledgments

This work was supported by Akademiska Hus, Göteborg Energi AB, Valmet Power AB, the Swedish Energy Agency, the Swedish Gasification Center (SFC), and The Centre for Combustion Science and Technology (CECOST). The computations were performed using the resources of the Chalmers Centre for Computational Science and Engineering (C3SE), provided by the Swedish National Infrastructure for Computing (SNIC). The authors thank Martin Seemann for his contributions to the experimental work and research engineers Jessica Bohwalli, Rustan Marberg, and Johannes Öhlin for technical assistance.

Notation

Symbols

B = terminal velocity correlation parameter
C = concentration
C_D = drag coefficient
d = diameter
e_{ss} = coefficient of restitution for particle collisions
$\boldsymbol{g}$ = gravitational acceleration vector
$g_{0,ss}$ = radial distribution function
$\boldsymbol{I}$ = identity matrix
I_{2D} = second invariant of the deviatoric stress tensor
K = interphase momentum exchange coefficient
$\dot{m}$ = mass flow rate
ΔP = pressure difference
p = (shared) pressure
p_s = solids pressure
Re = Reynolds number
t = time
$\boldsymbol{u}$ = velocity vector
$u_{r,s}$ = terminal velocity for the solid phase

$\dot{V}$ = volumetric flow rate
X = mass fraction
α = volume fraction
$\alpha_{s,max}$ = maximum packing limit of the solid phase
Θ = granular temperature
λ = bulk viscosity
μ = shear viscosity
ρ = density
τ = stress-strain tensor
ϕ = angle of internal friction

Subscripts

All = main steam duct (cf. Figure 3)
col = collisional
fr = frictional
G = gasifier
g = gas phase
He = helium
i = loop seal indicator (LS1 or LS2)
kin = kinetic
LS1 = loop seal 1
LS2 = loop seal 2
s = solid phase
st = steam

Literature Cited

1. Kunii D, Levenspiel O. *Fluidization Engineering*, *Vol*. 2. Boston: Butterworth-Heinemann, 1991.
2. Kunii D, Kunugi T. Continuous carbonization and gasification of particulate coal with double recirculation of fluidized particulate heat carrier. US Patent 3,912,465. 1975.
3. van der Meijden CM. *Development of the MILENA Gasification Technology for the Production of Bio-SNG*. PhD Thesis. Eindhoven, The Netherlands: TU Eindhoven, 2010.
4. Schuster G, Löffler G, Weigl K, Hofbauer H. Biomass steam gasification - an extensive parametric modeling study. *Bioresour Technol*. 2001;77:71–79.
5. Lyngfelt A, Leckner B, Mattisson T. A fluidized-bed combustion process with inherent CO_2 separation: application of chemical-looping combustion. *Chem Eng Sci*. 2001;56:3101–3113.
6. Martínez A, Lara Y, Lisbona P, Romeo LM. Operation of a mixing seal valve in calcium looping for CO_2 capture. *Energy Fuels*. 2014; 28:2059–2068.
7. Martínez A, Lisbona P, Lara Y, Romeo LM. Energy intensity reduction of Ca-looping CO_2 capture by applying mixing loop seals and cyclonic systems. In: *Proceedings of the 13th International Conference on Multiphase Flow in Industrial Plants (MFIP13)*. Sestri Levante, Genova, Italy, 2014.
8. Basu P, Butler J. Studies on the operation of loop-seal in circulating fluidized bed boilers. *Appl Energy*. 2009;86:1723–1731.
9. Kumar Chandel M, Alappat BJ. Pressure drop and gas bypassing in recirculating fluidized beds. *Chem Eng Sci*. 2006;61:1489–1499.
10. Li Y, Lu Y, Wang F, Han K, Mi W, Chen X, Wang P. Behavior of gas-solid flow in the downcomer of a circulating fluidized bed reactor with a V-valve. *Powder Technol*. 1997;91:11–16.
11. Kim SW, Namkung W, Kim SD. Solids flow characteristics in loop-seal of a circulating fluidized bed. *Korean J Chem Eng*. 1999;16:82–88.
12. Kim SW, Namkung W, Kim SD. Solid recycle characteristics of loop-seals in a circulating fluidized bed. *Chem Eng Technol*. 2001; 24:843–849.
13. Kim SW, Kim SD. Effects of particle properties on solids recycle in loop-seal of a circulating fluidized bed. *Powder Technol*. 2002;124: 76–84.
14. Mayer K, Piesenberger S, Pröll T, Hofbauer H. The gas flow in the loop seals of a dual circulating fluidized bed: splitting of the fluidizing agent and gas leakage through the loop seals. In: *The 14th International Conference on Fluidization - From Fundamentals to Products*, *ECI Symposium Series*, Noordwijkerhout, The Netherlands, 2013.
15. Seo MW, Nguyen TDB, Lim YI, Kim SD, Park S, Song BH, Kim YJ. Solid circulation and loop-seal characteristics of a dual circulating fluidized bed: experiments and CFD simulation. *Chem Eng J*. 2011;168:803–811.
16. Lind F, Seemann M, Thunman H. Evaluation of fluid dynamics in a hot and a cold system of interconnecting fluidised beds. In: *International Conference on Fluidization, Fluidization XIII*. Gyeong-ju, Korea: ECI Digital Archives, 2010:869–876.
17. Larsson A, Israelsson M, Lind F, Seemann M, Thunman H. Using ilmenite to reduce the tar yield in a dual fluidized bed gasification system. *Energy Fuels*. 2014;28:2632–2644.
18. Larsson A, Seemann M, Neves D, Thunman H. Evaluation of performance of industrial-scale dual fluidized bed gasifiers using the Chalmers 2–4-MWth gasifier. *Energy Fuels*. 2013;27:6665–6680.
19. Lind F. *Design and Operation of a Chemical-Looping Reformer for Catalytic Upgrading of Biomass-Derived Gas*. PhD Thesis. Gothenburg, Sweden: Chalmers Univiersity of Technology, 2013.
20. Glicksman LR, Hyre MR, Farrell PA. Dynamic similarity in fluidization. *Int J Multiphase Flow*. 1994;20:331–386.
21. Snider DM. An incompressible three-dimensional multiphase particle-in-cell model for dense particle flows. *J Comput Phys*. 2001; 170:523–549.
22. Hadjiconstantinou NG, Garcia AL, Bazant MZ, He G. Statistical error in particle simulations of hydrodynamic phenomena. *J Comput Phys*. 2003;187:274–297.
23. Benyahia S, Sundaresan S. Do we need sub-grid scale corrections for both continuum and discrete gas-particle flow models? *Powder Technol*. 2012;220:2–6.
24. Leckner B, Golriz MR, Zhang W, Andersson BA, Johnsson F. Boundary layers-first measurements in the 12 MW CFB research plant at Chalmers University. In: *International Conference on Fluidized Bed Combustion*, New York, USA: ASME, 1991:771–776.
25. Thunman H, Åmand LE, Leckner B, Johnsson F. A cost effective concept for generation of heat, electricity and transport fuel from biomass in fluidized bed boilers – using existing energy infrastructure. In: *Proceedings of the 15th European Biomass Conference & Exhibition - From Research to Market Deployment*. Berlin, Germany, 2007.
26. Feng YQ, Xu BH, Zhang SJ, Yu AB, Zulli P. Discrete particle simulation of gas fluidization of particle mixtures. *AIChE J*. 2004;50: 1713–1728.
27. Zhou ZY, Yu AB, Zulli P. Particle scale study of heat transfer in packed and bubbling fluidized beds. *AIChE J*. 2009;55:868–884.
28. Kriebitzsch SHL, van der Hoef MA, Kuipers JAM. Drag force in discrete particle models – continuum scale or single particle scale? *AIChE J*. 2013;59:316–324.
29. van Wachem BGM, Schouten JC, van den Bleek CM, Krishna R, Sinclair JL. Comparative analysis of CFD models of dense gas–solid systems. *AIChE J*. 2001;47:1035–1051.
30. van Wachem B, Sasic S. Derivation, simulation and validation of a cohesive particle flow CFD model. *AIChE J*. 2008;54:9–19.
31. Syamlal M, Rogers W, O'Brien TJ. *MFIX Documentation: Theory Guide*. Technical Note, DOE/METC-94/1004, NTIS/DE94000087. Springfield: National Technical Information Service, 1993.
32. Syamlal M, O'Brien TJ. Computer simulation of bubbles in a fluidized bed. *AICHE Symp Ser*. 1989;85:22–31.
33. Dallavalle J. *Micromeritics*. New York: Pitman, 1948.
34. Garside J, Al-Dibouni MR. Velocity-voidage relationships for fluidization and sedimentation in solid-liquid systems. *Ind Eng Chem Process Des Dev*. 1977;16:206–214.
35. Lun CK, Savage SB, Jeffrey DJ, Chepurniy N. Kinetic theories for granular flow: inelastic particles in Couette flow and slightly inelastic particles in a general flow field. *J Fluid Mech*. 1984;140: 223–222.
36. Ogawa S, Umemura A, Oshima N. On the equations of fully fluidized granular materials. *Z Angew Math Phys*. 1980;31:483–493.
37. Gidaspow D, Bezburuah R, Ding J. *Hydrodynamics of Circulating Fluidized Beds: Kinetic Theory Approach*. Chicago, IL: Department of Chemical Engineering, Illinois Institute of Technology, 1991.
38. Schaeffer DG. Instability in the evolution equations describing incompressible granular flow. *J Differ Equ*. 1987;66:19–50.
39. Nguyen TDB, Seo MW, Lim YI, Song BH, Kim SD. CFD simulation with experiments in a dual circulating fluidized bed gasifier. *Comput Chem Eng*. 2012;36:48–56.
40. Min J, Drake JB, Heindel TJ, Fox RO. Experimental validation of CFD simulations of a lab-scale fluidized-bed reactor with and without side-gas injection. *AIChE J*. 2010;56:1434–1446.
41. Xu J, Zhu JX. Experimental study on solids concentration distribution in a two-dimensional circulating fluidized bed. *Chem Eng Sci*. 2010;65:5447–5454.
42. Vasquez SA, Ivanov VA. *A Phase Coupled Method for Solving Multiphase Problems on Unstructured Meshes*. American Society of

Mechanical Engineers, Boston, USA: Fluids Engineering Division (Publication), 2000;251:743–748.
43. Desantes JM, Payri R, Salvador FJ, Gil A. Development and validation of a theoretical model for diesel spray penetration. *Fuel*. 2006; 85:910–917.
44. Cloete S, Johansen ST, Amini S, Grid independence behavior of fluidized bed reactor simulations using the two fluid model: effect of particle size. *Powder Technol*. 2015;269:153–165.
45. van Ommen JR, Teuling M, Nijenhuis J, van Wachem BGM. Computational validation of the scaling rules for fluidized beds. *Powder Technol*. 2006;163:32–40.
46. Zhang DZ, VanderHeyden WB. High-resolution three-dimensional numerical simulation of a circulating fluidized bed. *Powder Technol*. 2001;116:133–141.
47. Gel A, Li T, Gopalan B, Shahnam M, Syamlal M. Validation and uncertainty quantification of a multiphase computational fluid dynamics model. *Ind Eng Chem Res*. 2013;52: 11424–11435.
48. Galvin JE, Benyahia S. The effect of cohesive forces on the fluidization of aeratable powders. *AIChE J*. 2014;60:473–484.

Manuscript received Oct. 7, 2014, and revision received Feb. 10, 2015.